IEEE Photonics Journal
An IEEE Photonics Society Publication

Open Access

An Improved Optical Fiber Remote Sensing Method Based on Polarized Low-Coherence Interferometry

Volume 10, Number 1, February 2018

Kun Liu
Dongdong Ju
Shuang Wang
Junfeng Jiang
Mengnan Xiao
Xue Wang
Tiegen Liu

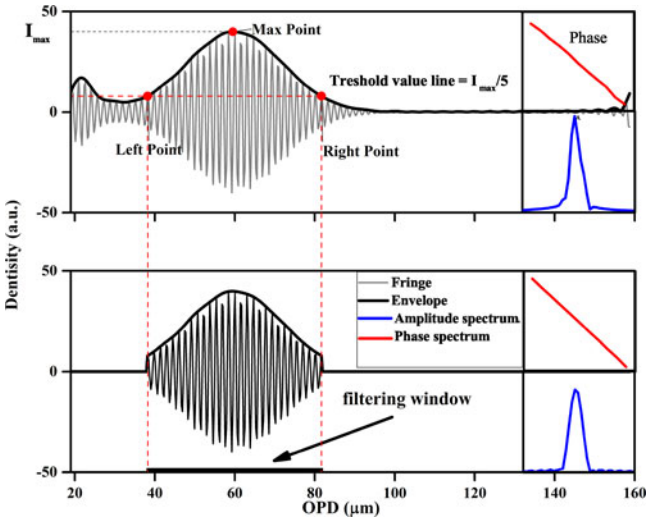

DOI: 10.1109/JPHOT.2017.2785124
1943-0655

An Improved Optical Fiber Remote Sensing Method Based on Polarized Low-Coherence Interferometry

Kun Liu, Dongdong Ju, Shuang Wang, Junfeng Jiang, Mengnan Xiao, Xue Wang, and Tiegen Liu

College of Precision Instrument and Optoelectronics Engineering, Tianjin University Key Laboratory of Optoelectronics Information Technology, MEC, Tianjin 300072, China

DOI:10.1109/JPHOT.2017.2785124

Manuscript received October 9, 2017; revised December 8, 2017; accepted December 13, 2017. Date of publication December 19, 2017; date of current version January 5, 2018. This work was supported in part by the National Natural Science Foundation of China under Grant 61505139, Grant 61735011, Grant 61675152, Grant 61378043, and Grant 61475114, in part by the Tianjin Natural Science Foundation under Grant 16JCQNJC02000, in part by the National Instrumentation Program of China under Grant 2013YQ030915, in part by the open project of Key Laboratory of Opto-electronics Information Technology under Grant 2017KFKT003 and Grant 2017KFKT004), in part by the open project of Key Laboratory of Micro Opto-electro Mechanical System Technology under Grant MOMST2016-3, in part by the Ministry of Education, and in part by the Seed Foundation of Tianjin University. Corresponding author: Shuang Wang (e-mail: sarahwang02166@gmail.com).

Abstract: We proposed an improved phase-based method by using a filtering window on the low-coherence interferogram. Through theoretical derivation and numerical simulation, we prove the correction of our proposed method that the fringe phase can be demodulated nondestructively after applying a symmetrical filtering window nearby the envelope peak, and our method can enhance system SNR. Since fringe overlap phenomenon arising from narrow bandwidth occurs frequently in single-mode sensing system, this method is especially applicable to remote sensing wherein the localization of interference fringe is difficult using traditional phase-based methods. To verify this method, an experiment with a single-mode fiber Fabry-Perot air pressure sensing system was carried out. The experiment results showed that the precision using our method decreased to less than 0.053% in full 280 kPa pressure scale and the sensing distance extended to 20 km, which were apparently superior to traditional phase-based methods.

Index Terms: Remote sensing and sensors, image analysis.

1. Introduction

The low-coherence interferometry (LCI) plays a crucial role in coherence scanning interferometry [1], optical coherence tomography [2] and probing cellular morphology [3] owing to the ability of absolute measurement with sub-micrometer resolution. Low-coherence interferogram can be demodulated using either fringe localization alone or in combination with fringe phase. Since 1992, many fringe-pattern-based algorithms [4]–[6] and phase-based algorithms have been proposed in succession to achieve high-precision demodulation. Phase-based algorithms (e.g., spatial frequency domain analysis [7] phase-crossing algorithm [8], absolute phase recovery algorithm [9]) characterize the measured quantity with phase rather than pure intensity characteristic. Deservedly they get higher precision than fringe-pattern-based algorithms and has many advantages such as immunity to the light intensity fluctuation and wavelength drift and compatible with down-sample [10].

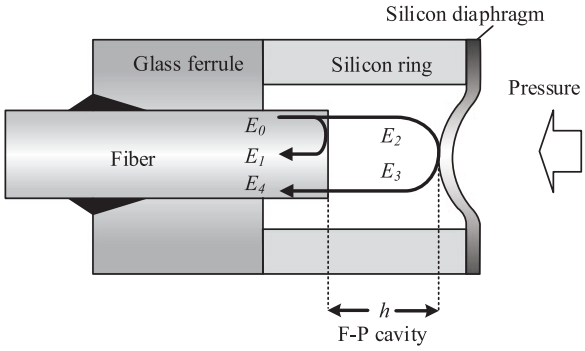

Fig. 1. The structure of the optical fiber air pressure sensor.

All above phase-based algorithms essentially are based on a premise that the source is wide-spectrum emitting a wavelength range over 100 nm, in which case the first-order fringe and the zero-order fringe are completely separated [11]. However, in many applications such as aviation, deep sea and oil well detection, muti-mode transmission can far from satisfy remote sensing and single-mode transmission is imperative. The attendant problem in single-mode transmission is, the bandwidth of common commercial broadband light source centered at 1310 nm or 1550 nm is only about 5 $\sim$ 100 nm. In our previous studies, we found that the deeper the cavity length of sensors are, the worse the linearity degree of itself will become. The possible reason is that the flatness of bottom surface is getting lower and lower with the increase in corrosion depth. Unfortunately, the limits of light source bandwidth and cavity length jointly constrained the implementation of phase-based algorithms in SMF low-coherence sensing system. For source having a Gaussian spectral distribution, the fringe period number is proportional to the center wavelength and inversely proportional to FWHM. Generally, the typical broadband light source is supposed to have a coherence length of about a few micrometers to ensure that the period number isn't too large (i.e., less than 20), otherwise this interferogram will be very different from typical LCI interferogram. For a typical phosphor-based LED with a center wavelength of 578 nm and a FWHM of 150 nm, its period number is 8. However, for a typical SLED with a center wavelength of 1550 nm and a FWHM of 100 nm, the period number will increase significantly to 31. It means in single-mode system, a wider range of fringe will damage the fringe's integrity when the measurand parameter is an inappropriate value. If performing phase-based algorithm to the damaged fringe directly without any preprocessing in the spatial domain, there will occur poor linearity even jump errors. So considering the requirement of high precision and large measurement range in remote sensing, we proposed an improved method based on polarized low-coherence interferometry (PLCI). The core idea of our method is to apply a symmetry filtering window to the fringe nearby its highest point before frequency transformation.

In this Letter, we designed a long distance SMF F-P air pressure sensing system based on PLCI. Absolute phase recovery algorithm combined with our proposed filtering window is adopt. The experimental results showed that, in single-mode sensing system, comparing with traditional absolute phase recovery algorithm, our proposed method avoided jump errors, enhanced SNR and improved demodulation precision in a wider measurement region and in a longer sensing distance.

2. Principles

2.1 Optical Fiber Air Pressure Sensor Based on F-P Interferometer

The structure of the optical fiber air pressure sensor based on F-P interferometer is depicted in Fig. 1. It consists of SMF, glass ferrule, silicon ring, and silicon diaphragm. The silicon diaphragm is elastic which serves as the pressure sensing element. The F-P cavity isn't vacuum-sealed, its linearity error arising from residual pressure is about 0.006%. Therefore, silicon diaphragm's deformation is thought to has a linear relationship with pressure, we can demodulate the cavity

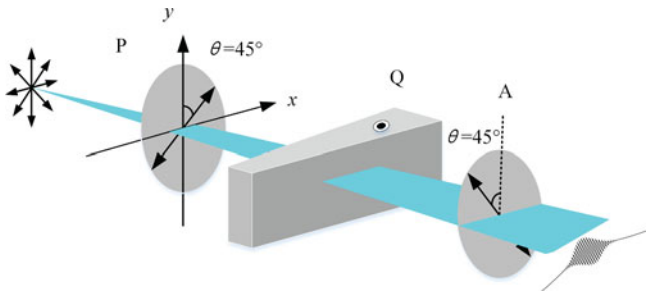

Fig. 2. The schematic diagram of PLCI.

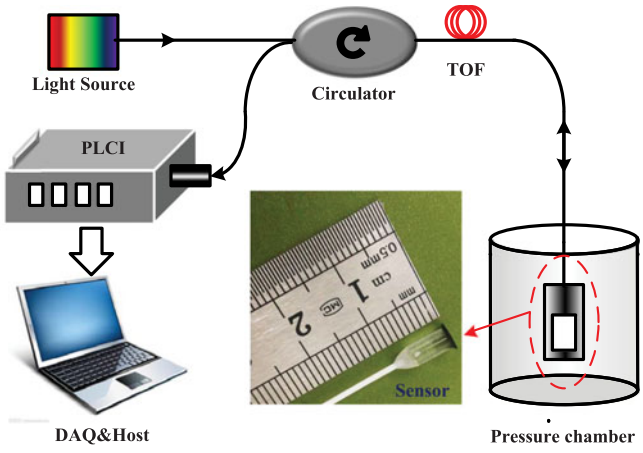

Fig. 3. The diagram of remote SMF F-P air pressure sensing system based on PLCI.

length to acquire the pressure. Assuming light is plane wave and ignoring all kinds of loss, the back-reflected light can approximately be expressed as two beam interference when the intensity of two beam reflected light is equal. Output light can be formulized as

$$I = |E_1 + E_4|^2 = \left|E + E e^{-j(2kh+\pi)}\right|^2 = I_0 [1 - \cos(2kh)] \tag{1}$$

where k stands for the wave number of broadband light, h is the cavity length.

2.2 PLCI

The PLCI demodulation module is composed of the polarizer, the birefringent wedge and the analyzer shown as Fig. 2. The polarization directions of polarizer and analyzer are vertical to each other, and 45° angle to optical axis of the wedge. The wedge's refractive index $n = |n_o - n_e|$ is the difference between extraordinary light and ordinary light. PLCI is actually a cross-polarized system. When considering the consistency of the birefringent, output light can be write as

$$I = \left|-E_0 \sin(45^\circ) e^{jknd} \sin(45^\circ) + E_0 \cos(45^\circ) \cos(45^\circ)\right|^2 = I_0 [1 - \cos(knd)] \tag{2}$$

2.3 Sensing System and Absolute Phase Recovery Algorithm

Fig. 3 is remote SMF F-P air pressure sensing system diagram. Broadband light source used in system is SLED, whose power spectrum is nearly Gaussian distribution. Through single-mode transmission optical fiber (TOF), the broadband light reaches to the sensor. The sensor is sealed in an air pressure chamber to sense external pressure. Then the reflected light carrying pressure information propagates into PLCI system through TOF again. The PLCI system scan continuously

the optical path difference (OPD) introduced by the sensor. Finally, the detector will appear low-coherence interferogram near those areas where the OPD generated by the wedge is equal to twice of the cavity length. In the following derivation, we merged refractive index n into d. So the interferogram forming on the detector can be formulized as

$$I(d, h) = \int_{-\infty}^{\infty} C(k)\,[1 - \cos(2kh)]\,[1 - \cos(kd)]\,dk \tag{3}$$

where d presents the OPD corresponding to the number of pixels. And $C(k)$ denotes the transmission coefficient in the whole system including light spectrum, transmission loss and detector sensing sensitivity. Expanding (3) and ignoring DC term and those terms invisible on detector results in the following (4)

$$I(d, h) = 2\int_{-\infty}^{\infty} C(k)\cos(kd)\,dk - \int_{-\infty}^{\infty} C(k)\cos[k(d - 2h)]\,dk \tag{4}$$

Here we mark the first term as the zero-order fringe and the second term as the first-order fringe. Analyzing the shape of the first-order fringe, its curve is symmetric distribution about the axis of $d = 2h$, and its distribution range is exactly twice of the coherence length L_C around the OPD where is equal to twice of the cavity length h. To acquire the phase information, we apply the Fourier transformation in the spatial variable d to (4)

$$F(j\omega, h) = \left[1 - \frac{1}{2}\exp(-j2\omega h)\right][C(\omega) + C(-\omega)] \tag{5}$$

It seems that its phase is not linear with h. But when zero-order fringe and first-order fringe is separated, we can change the relative position of the wedge and the detector to make the zero-order fringe invisible on the detector. If so, the Fourier transformation is following form

$$F(j\omega, h) = \frac{1}{2}\exp(-j2\omega h)\,[C(\omega) + C(-\omega)] \tag{6}$$

The Fourier transform has the following features: (1) The amplitude term is completely the same as the distribution form of SLED spectrum in wave vector domain. (2) The phase term, in contrast, completely irrelevant with SLED spectrum; there is a one-to-one correspondence between absolute phase and the angular frequency ω with a constant coefficient $2h$. As a result, the fringes absolute phase can be retrieved by selecting a monochromatic angular frequency ω_0, and then unfolding the warped phase in the $[-\pi, \pi]$ range.

3. Limits in SMF Sensing System and Improved Demodulation Method

If taking into consideration the bandwidth of light source in SMF sensing system and limited length of F-P sensor, (5) can't be deduced to (6) in most cases. Significant differences are obvious in Fig. 4. We can see the spread of fringe in SMF sensing system is much broader than that of using white LED. And due to MEMS crafts, the cavity length can't be corroded too deeply, otherwise the bottom surface of air cavity will become rough which result in the sensor itself poor linearity. Above two factors lead to that, the broad first-order fringe and the zero-order fringe will overlap when the silicon diaphragm deformation is large (i.e. cavity length is shorter than coherence length). To visualize above problem, a PLCI interferogram corresponding to the cavity length ranging from 30 μm to 70 μm and the coherence length set as 35 μm is simulated. The simulated interferogram and demodulation results using absolute phase recovery algorithm are shown in Fig. 5(a). For simplified representation, Fig. 5(a) only show three typical cases in which the first-order fringe is defective or the zero-order fringe is visible. We see there exsits a severe level jump error, and its measurement range and precision is small. From Fig. 5(c), we can figure out the internal mechanism of the result in Fig. 5(a), the linearity between wrapped phase and angular frequency is distorted owing to the exist of zero-order fringe. The simulation results consistent with theoretical expectations.

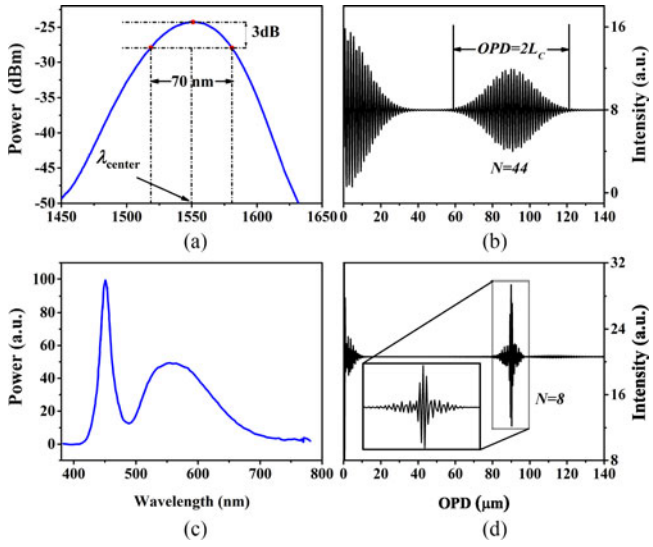

Fig. 4. Typical LCI interferograms with different broadband light sources under same system parameter configuration. Panel (a) is the density spectrum of 1550 nm SLED, panel (b) is the interferogram with SLED, panel (c) is the density spectrum of white LED, panel (d) is the interferogram with LED.

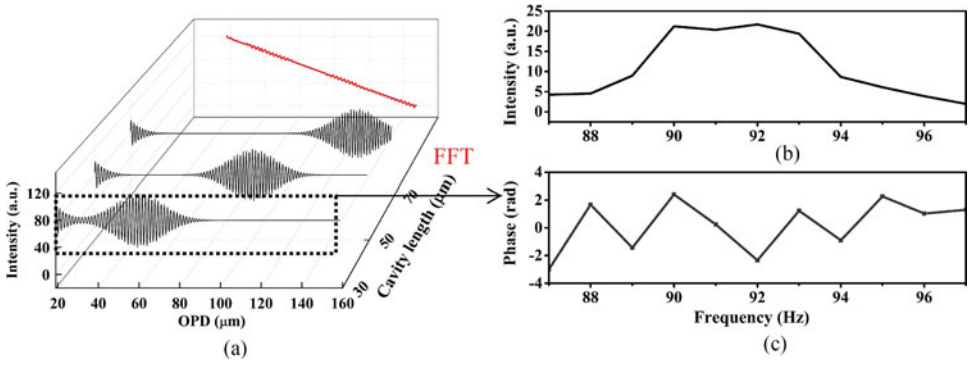

Fig. 5. Panel (a) is the simulated interferogram ranging from 30 μm to 70 μm, wherein the red line is the demodulated absolute phase, and its amplitude is rescaled to display in the same figure with interference fringes. Panel (b) is amplitude spectrum and panel (c) is wrapped phase spectrum.

To perform the phase-based algorithm normally on those jump points, we noticed that the first-order fringe, as we referred to above, is supposed to be symmetric even function with the vertical axis $d = 2h$ through the highest point of the envelope. In the case of overlap or defective not serious, if we apply a length appropriate filtering window whose central axis is $d = 2h$ to first-order fringe that the first-order fringe in the window is separated with zero-order fringe, the phase-based algorithm may be still performed normally and robustly. To illustrate the correctness of our hypothesis, we have the following derivation process. The first-order fringe is the following form after applied a filtering window

$$\begin{aligned} I^{W}(d,h) &= I(d,h)\, g_{\tau}(d-2h) \\ &= \int_{-\infty}^{\infty} C(k)\cos[k(d-2h)]\, g_{\tau}(d-2h)\, dk + \int_{-\infty}^{\infty} C(k)\cos(kd)\, g_{\tau}(d-2h)\, dk \\ &= \int_{-\infty}^{\infty} [C(k)\cos(kd)\, g_{\tau}(d)] * \delta(d-2h)\, dk \end{aligned} \tag{7}$$

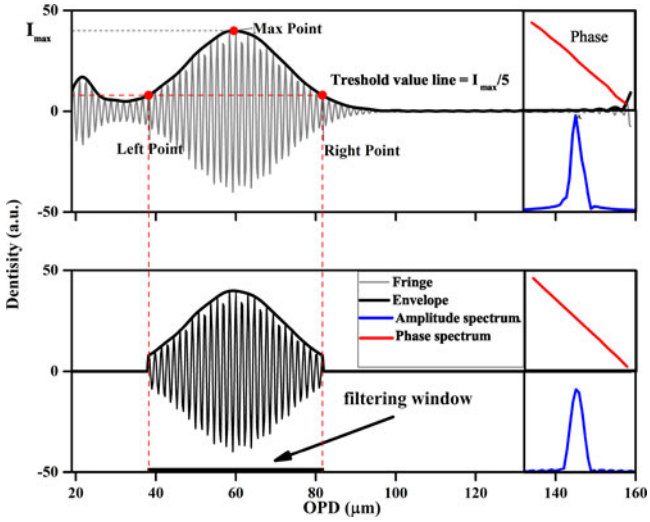

Fig. 6. The implementation steps of proposed method. The red subgraph represents the phase spectrum of Fourier transform and the blue subgraph represents the amplitude spectrum of Fourier transform.

where the term $g_\tau(d-2h)$ represents the filtering window whose length is τ and central position is $d=2h$. Here, the filtering window has filtered out the zero-order fringe totally. The Fourier transform of (7) is

$$F^W(j\omega, h) = \exp(-2j\omega h)\int_{-\infty}^{\infty} \mathcal{F}\{C(k)\cos(kd)\, g_\tau(d)\}\mathrm{d}k \tag{8}$$

We know that the Fourier transform of both real and even function is a real and even function. It is apparent that the term $C(k)\cos(kd)\, g_\tau(d)$ is a real even function in terms of d, so the Fourier transform $\mathcal{F}\{C(k)\cos(kd)\, g_\tau(d)\}$ is a real number which won't introduce additional phase factor. Thus the absolute phase is still linear proportional to the cavity length h. Therefore, the defective interferogram can still be used for demodulation using phase-based algorithms after applying a filtering window. In theory, the window can be any form of a symmetric distribution such as rectangle window, hanning window, hamming window and so on, as long as term $\mathcal{F}\{C(k)\cos(kd)\, g_\tau(d)\}$ is even function. We have simulated different window functions, results showed demodulation precision varied less than 5%. Therefore, we select the simplest rectangular window as the window function. The procedure of our proposed algorithm can be summarized in the following steps shown as Fig. 6

1) Apply Fourier transform to the interferogram then filter its high frequency component and low frequency component, where the high frequency component signify various forms of noise, and the low frequency DC component indicate the gaussian-distribution background.
2) Apply the inverse Fourier transform to the above filtered amplitude term. Its real part represents the filtered fringes and its module represents the envelope of the filtered fringes.
3) Mark the highest point of the envelope as Max Point, then we set an appropriate threshold between 1/6 and 1/3 of envelope peak to the filtered fringes, then find left point and right point in the envelope curve corresponding to the threshold respectively. The filtering window is exactly the interval from the left point to the right point.
4) Perform phased-based algorithm to the filtered interferogram.

In fact, compared with window form, window size is a more important factor controlling the overall demodulation error. The interferogram can be decomposed into noise item and ideal interferogram item. White noise is evenly distributed in whole Fourier spectrum. When performing absolute phase recovery algorithm, the phase of noise coupled into the phase spectrum of interferogram is the main source of demodulation error. By adding a filter window, the noise outside the window can be completely filtered so as to improve the overall SNR. Therefore, our proposed method can enhance

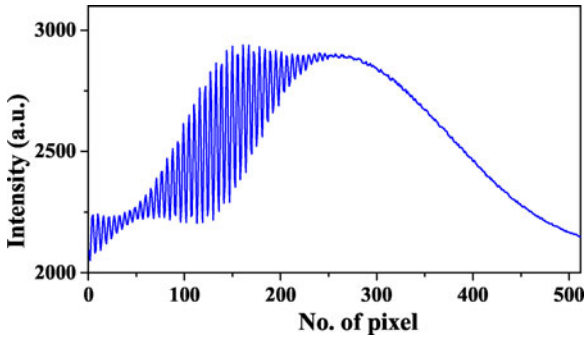

Fig. 7. Raw interferogram.

system SNR and reduce the demodulation error. The increase in SNR is directly decided by ratio K of window size with the overall size of the interferogram. To optimize window size, the threshold is set between 1/6 and 1/3 of envelope peak. This is because when the threshold is too small, it is hard to separate overlapped fringes. On the contrary, PLCI system itself exists non-vertical incident dispersion [12] and optical wedge position dispersion [13] which will make the fringe asymmetry. If the window size is too narrow, too less data will increase the demodulation error in turn. In SMF interferogram, the ratio K is about 1/3, so the SNR of interferogram increase by 5 dB using our proposed method.

$$\mathrm{SNR}' = 10\log\left(\frac{P_{\mathrm{signal}}}{K\,P_{\mathrm{noise}}}\right) = \mathrm{SNR} - 10\log(K) = \mathrm{SNR} + 5 \tag{9}$$

4. Experimental Results

To verify the effectiveness of our proposed method, we set up a remote SMF Fabry-Perot (F-P) air pressure sensing system shown as Fig. 3. In our system, a birefringent wedge made of α-BBO with a 5° inclination is used to ensure the fringes are not overly dense and the measurement range is sufficient. The air pressure sensor in experiment is hand-made which isn't sealed into vacuum, its cavity is about 35 μm to close to that of sensors made by MEMS crafts. The detector arrays has 512 pixels, and the pixel pitch is 25 μm, whose sample interval corresponding to OPD is 0.2629 μm. The maximum power of the SLED is 14 mW whose spectrum is shown as Fig. 4(a). A coil of theoretical limit 20 km SM-28e+ fiber is inserted between the sensor and demodulation module. In our experiment, we increased the air pressure from 3 kPa to 283 kPa at intervals of 10 kPa by controlling the air pressure chamber. When applying maximum pressure 283 kPa on the sensor, the raw interferogram is shown as Fig. 7.

Applying improved demodulation method (hereinafter, the Imp.)and conventional absolute phase recovery algorithm (hereinafter, the Con.)respectively to demodulate the interferogram. Here we set the threshold as 1/4 of envelope peak. Fig. 8 shows the demodulation results of relations between absolute phase and pressure. Demodulation results show significant differences between these two methods. The line by using of the Con. is apparently not linear in full pressure scale, it is because some measuring points drift out of the orders they should be in owing to overlap phenomenon. As a clear contrast, the absolute phase with Imp. method changes linearly with pressure, and its is predictable that there wont occur jump error in larger range. Compared with Con., our proposed method possesses a larger measurement range.

Linear fitting the absolute phase with pressure to acquire the demodulation precision, we get the absolute phase by using of Imp. shows good linearity of 0.9999 with a full scale maximum error 0.15 kPa. The linear region with Con. is only 150 kPa. Thus, if we perform Con. directly in above 150 kPa linear region, the maximum error is 0.36 kPa which is even larger than 0.15 kPa in 283 kPa full pressure scale using our method. Experiment results with two methods are shown as Table 1, The demodulation error with our proposed method is about half of that with conventional algorithm,

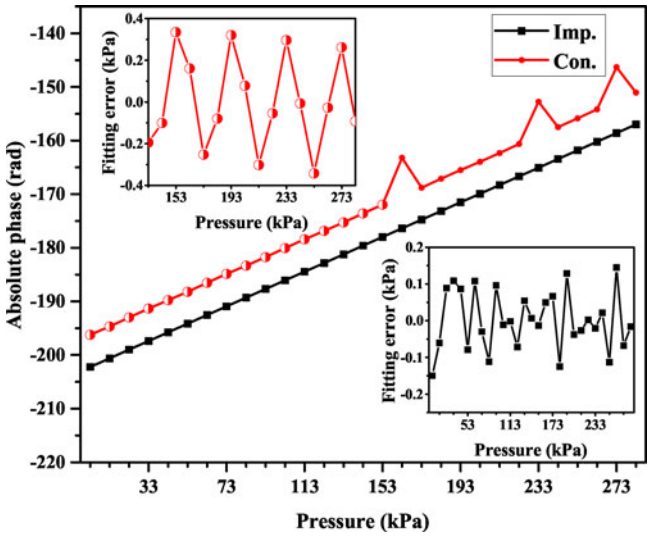

Fig. 8. Relation between the absolute phase and air pressure. Black line (i.e., Imp.) represents improved algorithm; red line (i.e., Con.) represents absolute phase recovery algorithm.

TABLE 1
Experiment Results With Different Algorithms

Measure Range (kPa)	Method	Error (kPa)	F.S. Error (%)
150	Con.	0.36	0.24
	Imp.	0.13	0.08
280	Con.	–	–
	Imp.	0.15	0.053

which proved that our proposed method has effect on enhancing system SNR and reducing the demodulation error. Meanwhile the experiments results without jump error verified the effectiveness of our proposed method could help reconstruct distorted phase of overlapping fringes.

The fitting error 0.15 kPa corresponds to demodulation precision 0.053% in full 280 kPa. As we have mentioned before, the air pressure sensors linearity error arising from residual pressure is about 0.006% which is much smaller than the experimental results. Therefore, most of the experiment error is caused by nonlinearity of diaphragm response, instability of PLCI demodulation system and inherent error of demodulation method. In our early local muti-mode pressure sensing system research, the maximum precision is 0.08%. Its apparent that the remote single-mode sensing system combined with our proposed method shows excellent features than muti-mode sensing system not only in terms of measurement range, transmission distance, but also in demodulation precision.

5. Conclusion

In summary, we present an improved phase-based method adding a filtering window on overlapping fringes before recovering absolute phase for SMF remote air pressure sensing system. This method is effective on reconstructing the distorted phase information and enhancing the SNR, thus expands

greatly the application range of phase-based algorithm. In our experiment, the transmission distance 20 km is achieved, which has the potential to be used for the remote sensing filed such as aviation, deep sea and oil well detection. And the error is less than 0.053% in full 280 kPa scale.

References

[1] B. S. Lee and T. C. Strand, "Profilometry with a coherence scanning microscope," *Appl. Opt.*, vol. 29, no. 26, pp. 3784–3788, 1990.

[2] E. A. Swanson *et al.*, "In vivo retinal imaging by optical coherence tomography," *Opt. Lett.*, vol. 18, no. 21, pp. 1864–1866, 1993.

[3] V. Backman *et al.*, "Measuring cellular structure at submicrometer scale with light scattering spectroscopy," *IEEE J Sel. Topics Quantum Electron.*, vol. 7, no. 6, pp. 887–893, Nov./Dec. 2001.

[4] G. Gianto, F. Salzenstein, and P. Montgomery, "Comparison of envelope detection techniques in coherence scanning interferometry," *Appl. Optic.*, vol. 55, no. 24, pp. 6763–6774, 2016.

[5] S. Wang *et al.*, "A simple and effective demodulation method for polarized low-coherence interferometry," *IEEE Photon. Technol. Lett.*, vol. 24, no. 16, pp. 1390–1392, Aug. 2012.

[6] K. G. Larkin, "Efficient nonlinear algorithm for envelope detection in white light interferometry," *J. Opt. Soc. Amer.*, vol. 13, no. 4, pp. 832–843, 1996.

[7] P. de Groot and L. Deck, "Surface profiling by analysis of white-light interferograms in the spatial frequency domain," *J. Mod. Optic.*, vol. 42, no. 2, pp. 389–401, 1995.

[8] M. E. Pawłowski, Y. Sakano, Y. Miyamoto, and M. Takeda, "Phase-crossing algorithm for white-light fringes analysis," *Opt. Commun.*, vol. 260, no. 1, pp. 68–72, 2006.

[9] J. Jiang *et al.*, "A polarized low-coherence interferometry demodulation algorithm by recovering the absolute phase of a selected monochromatic frequency," *Opt. Exp.*, vol. 20, no. 16, pp. 18117–18126, 2012.

[10] P. de Groot and L. Deck, "Three-dimensional imaging by sub-Nyquist sampling of white-light interferograms," *Opt. Lett.*, vol. 18, no. 17, pp. 1462–1464, 1993.

[11] W. Drexler *et al.*, "In vivo ultrahigh-resolution optical coherence tomography," *Opt. Lett.*, vol. 24, no. 17, pp. 1221–1223, 1999.

[12] T. Liu *et al.*, "Nonperpendicular incidence induced Sspatial frequency drift in polarized low-coherence interferometry and its compensation," *IEEE Photon. J.*, vol. 7, no. 6, Dec. 2015, Art. no. 2600807.

[13] S. Wang *et al.*, "Birefringence-dispersion-induced frequency domain nonlinearity compensation for polarized low-coherence interferometry demodulation," *IEEE Photon. Technol. Lett.*, vol. 33, no. 23, pp. 4842–4848, Dec. 2015.